PCCP

PAPER

View Article Online
View Journal | View Issue

# Electronic and optical properties of silicon based porous sheets

Cite this: *Phys. Chem. Chem. Phys.*, 2014, **16**, 16832

Yaguang Guo,[ab] Shunhong Zhang[ab] and Qian Wang*[ab]

Received 6th April 2014,
Accepted 12th June 2014

DOI: 10.1039/c4cp01491j

www.rsc.org/pccp

Si based sheets have attracted tremendous attention due to their compatibility with the well-developed Si-based semiconductor industry. On the basis of state-of-the-art theoretical calculations, we systematically study the stability, electronic and optical properties of Si based porous sheets including g-$Si_4N_3$, g-$Si_3N_4$, g-$Si_3N_3$ and g-$Si_3P_3$. We find that the g-$Si_3N_3$ and g-$Si_3P_3$ sheets are thermally stable, while the g-$Si_4N_3$ and g-$Si_3N_4$ are unstable. Different from the silicene-like sheets of SiN and $Si_3N$ which are nonplanar and metallic, both the porous g-$Si_3N_3$ and g-$Si_3P_3$ sheets are planar and nonmetallic, and the former is an indirect band gap semiconductor with a band gap of 3.50 eV, while the latter is a direct band gap semiconductor with a gap of 1.93 eV. Analysis of the optical absorption spectrum reveals that the g-$Si_3P_3$ sheet may have applications in solar absorbers owing to its narrow direct band gap and wide range optical absorption in the visible light spectrum.



The study of two dimensional (2D) monolayer materials has been a topic of high interest since the discovery of graphene[1] showing superior physical and chemical properties.[2] Among them, graphitic carbon nitrides $C_3N_3$, $C_3N_4$ and $C_4N_3$ catch considerable attention due to their novel mechanical, electronic, magnetic, and photocatalytic behaviors.[3–9] For example, Xie's group reported the first finding of a carbon nitride with graphite-like lamellar structure.[10] Li *et al.* synthesized a single layer of carbon nitride sheet labeled as g-$C_3N_3$ through the reaction of $C_3N_3Cl_3$ and Na by a simple solvothermal method.[11] Chai *et al.* found that g-$C_3N_3$ can exhibit optical absorption anisotropy and it may be used as a photocatalyst to split water.[12] Qiu *et al.* suggested that if each of the carbon atoms in g-$C_3N_3$ adsorbs a hydrogen atom, the hydrogenated structure (g-$H_3C_3N_3$) can display ferromagnetic properties with 100% half-metallicity around Fermi energy.[13] Ma *et al.* observed that g-$C_3N_3$ monolayer has high $H_2$ permeability and selectivity with a potential for $H_2$ purification.[14] Since silicon is in the same group as carbon in the periodic table, some intriguing questions arise: if C is replaced by Si, are these 2D Si–N sheets still stable? What properties do they have?

In fact, three dimensional (3D) Si–N materials are found to have some unique properties. Silicon nitride ($Si_3N_4$) is a light, hard, and strong engineering ceramic[15] at high temperatures, and it has high strength applications owing to its outstanding mechanical features.[16,17] There are two common forms of silicon nitride: α-$Si_3N_4$ and β-$Si_3N_4$. Both of them have hexagonal structures, but different in stacking modes.[18] Theoretical studies were carried out to explore the electronic structures, charge distribution, charge transfer and optical properties of these two phases.[19,20] In 1999 a new phase, labeled as c-$Si_3N_4$, was successfully synthesized[21] and first-principles calculations suggested its hardness being comparable to that of the hardest known oxide.[22] Although great efforts have been made to study 3D Si–N materials, less attention is paid to 2D Si–N sheets. Very recently silicene-like sheets of SiN and $Si_3N$ were investigated theoretically[23] and both of them were found to exhibit metallic behaviors but have different geometries: SiN sheets prefer the washboard-like buckled conformation, while $Si_3N$ sheets have chair-like buckled conformation. To the best of our knowledge there are no studies reported on 2D porous Si–N sheets like g-$Si_3N_3$, g-$Si_3N_4$, and g-$Si_4N_3$. In this paper, we systematically study the stability, electronic and optical properties of these designed 2D sheets.

First principles calculations were carried out by using density functional theory (DFT) as implemented in the Vienna ab initio Simulation Package (VASP code).[24] The electronic exchange–correlation functional was treated using the generalized gradient approximation (GGA) with Perdew–Burke–Ernzerhof (PBE) parametrization.[25] The interactions between electrons and nuclei were treated using projected augmented wave (PAW) potentials. Hybrid functionals in the Heyd–Scuseria–Ernzerhof (HSE06) form[26] were also used to achieve greater accuracy of the electronic and optical absorption properties. The energy cutoff was set at 500 eV. The convergence criteria for energy and force were set as 0.0001 eV and 0.01 eV $Å^{-1}$, respectively. The Brillouin zones were represented with 9 × 9 × 1 Monkhorst–Pack special

[a] *HEDPS, Center for Applied Physics and Technology, College of Engineering, Peking University, Beijing 100871, China. E-mail: qianwang2@pku.edu.cn*
[b] *Department of Materials Science and Engineering, College of Engineering, Peking University, Beijing 100871, China*

 

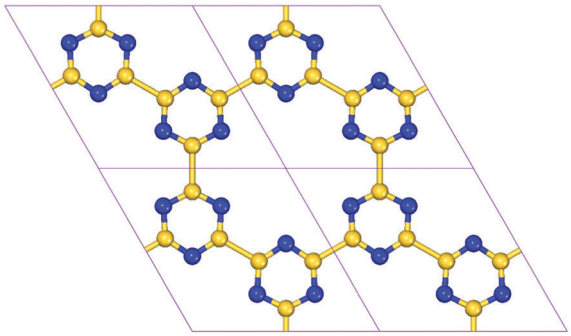

Fig. 1 Optimized structure of the g-$Si_3N_3$ sheet. Si and N atoms are represented by yellow and blue balls, respectively. The unit cells are marked by purple rhombus.

*k*-point meshes.[27] The vacuum space in the normal direction of the sheets was taken to be 20 Å, which is sufficient to avoid the interaction between the two neighboring layers. To confirm their dynamic stability, phonon calculations were performed using finite displacement method as implemented in the phonopy program.[28]

We first study a g-$Si_3N_3$ sheet where the initial geometry is generated from a g-$C_3N_3$ sheet by replacing C with Si. Fig. 1 shows the fully optimized geometrical structure which has a high symmetric space group of *P6/mmm* ($D^1_{6h}$, 191). The equilibrium lattice constant of the g-$Si_3N_3$ sheet is $a = b = 9.65$ Å, which is larger than the value of 7.11 Å of g-$C_3N_3$ sheet[13] and even larger than that of g-$C_4N_3$ sheet[9] due to the larger size of Si atoms and the porosity of this structure. The Si–Si and Si–N bond lengths in the ground state structure are 2.35 Å and 1.67 Å, respectively, indicating a feature of single σ bonds.

We then examine the stability of the g-$Si_3N_3$ sheet. To confirm its dynamic stability, we performed calculations of phonon spectra as displayed in Fig. 2(a), where no imaginary frequencies exist, indicating that the g-$Si_3N_3$ is dynamically stable. This is different from the cases of g-$Si_3N_4$ and g-$Si_4N_3$ which are found to be unstable from the calculations of phonon dispersions. The phonon instability of g-$Si_3N_4$ and g-$Si_4N_3$ implies that there might be some local distortion induced buckling in these nanosheets, which can be attributed to pseudo-Jahn–Teller distortion.[29] Such out-of-plane distortion has been suggested in previous studies on silicene[30] and g-$C_4N_3$.[3] Here, we focus only on the stable planar g-$Si_3N_3$ nanosheet. To further confirm the thermal stability of g-$Si_3N_3$ sheets at finite temperature, a larger 3 × 3 supercell containing 108 atoms was used to reduce the constraint of the lattice. *Ab initio* molecular dynamics (MD) simulations were carried out with a Nosé thermostat[31] at 300 K for 5000 steps with a time step of 1 fs. The fluctuations of total energy with simulation time are plotted in Fig. 2(b). After 5000 steps, we found that no obvious structure destruction occurred, and the average value of total energy remains nearly constant during the simulation, confirming that the g-$Si_3N_3$ is thermally stable at room temperature.

To compare the stability of g-$Si_3N_3$ with other silicon based sheets, we calculated the formation energy[32] of other 2D Si–N systems including SiN and $Si_3N$ sheets. The calculated results show that the formation energy of g-$Si_3N_3$ sheet (0.47 eV) is smaller than those of SiN sheet (1.02 eV) and $Si_3N$ (0.64 eV) sheets[23] due to its porosity, indicating that the g-$Si_3N_3$ sheet is energetically metastable. We note that the structural unit of g-$Si_3N_3$ is the $Si_3N_3$ ring. Therefore, this newly designed nanosheet could be synthesized by polymerization reaction using the synthesized $C_{21}H_{24}F_3N_3Si_3$ or $C_{12}H_{30}F_3N_3Si_3$ molecules which contain the hexagonal $Si_3N_3$ cores.[33,34] A similar procedure was reported to fabricate the g-$C_3N_3$ architectures.[11]

To study the electronic properties of the g-$Si_3N_3$ sheet, we calculated the electronic band structure and corresponding partial density of states (PDOS). The results are shown in Fig. 3(a) and (b), respectively. The g-$Si_3N_3$ sheet is found to be nonmagnetic due to zero spin polarization, while the silicene-like SiN structure is metallic resulting from the abundance of p-electrons of N elements, according to previous studies.[23] The band structure shows that the g-$Si_3N_3$ is an indirect band gap semiconductor with a band gap of 2.30 eV, because the valence band maximum (VBM) is located at the *Γ* point and the conduction band minimum (CBM) is located at the *K* point in the Brillouin zone. This is different from g-$C_3N_3$, which has a smaller direct band gap of 1.5 eV at the *K* point in the Brillouin zone.[13] We note that the VBM is quite flat, which would lead to

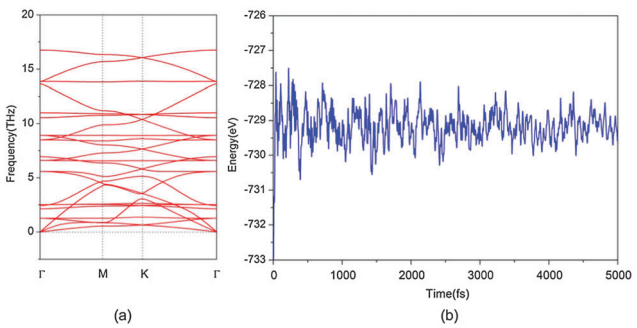


Fig. 2 (a) Phonon dispersions and (b) energy fluctuation with respect to time in MD simulations at 300 K for the g-$Si_3N_3$.

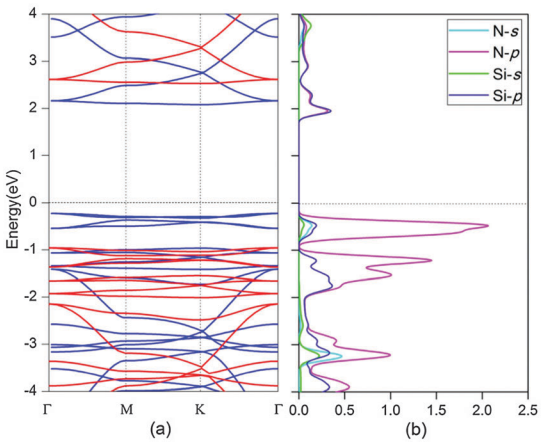


Fig. 3 (a) Electronic band structures of the g-$Si_3N_3$ calculated using GGA-PBE (blue lines) and HSE06 hybrid functional (red lines). (b) PDOS of the g-$Si_3N_3$ at GGA-PBE level. The Fermi energy level is shifted to 0.00 eV.

a large effective mass of holes. This can be understood from the fact that the tops of valence bands (VB) are comprised of the N 2p orbitals, as shown in Fig. 3(b). Previous studies on α- and β-$Si_3N_4$ phases manifested that both of them are semiconductors and the tops of their VB are also flat since they are derived from the more delocalized nonbonding N 2p orbitals,[19] indicating that the 2D and 3D Si–N systems have similar electronic properties to each other. As standard DFT calculations are well known to underestimate the band gap, we repeated the band structure calculations using the screened hybrid functional HSE06[26] which has been demonstrated to be more accurate in describing the exchange–correction energy of electrons. The results are also plotted in Fig. 3, showing both the GGA and HSE06 functionals lead to similar dispersion curves of the valence and conduction bands. However, the conduction bands are up-shifted, while the VB are down-shifted at the HSE06 level, resulting in a larger band gap of 3.50 eV, as compared to that obtained with the GGA. While the 3D α- and β-$Si_3N_4$ have band gaps at 4.63 and 4.96 eV,[19] respectively. Thus, we see that the electronic properties of Si–N based systems can be tuned by changing dimensionality.

Graphitic carbon nitrides are widely used for optical applications.[35,36] Therefore, it would be intriguing to investigate the optical properties of its new counterparts. We first study the optical absorption of the g-$Si_3N_3$ structure. The dielectric function is defined as $\varepsilon(\omega) = \varepsilon_1(\omega) + i\varepsilon_2(\omega)$, where $\varepsilon_1(\omega)$ and $\varepsilon_2(\omega)$ are the real and imaginary parts of the dielectric function, respectively. From the calculated $\varepsilon_2(\omega)$, we obtained the optical absorption curve, which is displayed in Fig. 4($a_1$). The curve shows a sharp increase at about 290 nm (corresponding photon energy is 4.30 eV), which originates from the π–π* electronic transitions. The wide absorption ranging from about 100 to 250 nm is derived from the electronic transitions between the inner non-bonding orbitals and π* orbitals. Compared with g-$C_3N_3$,[12] which has a main peak situated at 297 nm and a weak broad absorption from 78 to 114 nm, the g-$Si_3N_3$ also has a strong optical absorption in ultraviolet wavelengths but a wider range of optical absorption. Compared with the 3D $Si_3N_4$ system,[19] where the optical absorption curves for both α- and β-$Si_3N_4$ have three relatively sharp peaks around 113, 127 and 159 nm (corresponding photon energies are 11.0, 9.8 and 7.8 eV, respectively), the 2D g-$Si_3N_3$ undergoes a red shift. Thus, we see the effect of dimensionality on the optical properties in the Si–N based system. Usually, in a semiconductor, if the photon energy is greater than the band gap of the material, then electrons are excited onto the conduction bands. Thus there is an upper limit for wavelength, which is defined as $\lambda_{max} = 2\pi\hbar c/E_g$, where $\hbar$, $c$, and $E_g$ represent the Planck constant, light speed, and electronic band gap, respectively. The HSE06 calculations provide a band gap of 3.50 eV. Hence, as expected, all the absorption peaks are within the value of maximum light wavelength $\lambda_{max}$ of 355 nm, which is consistent with the calculated optical spectrum, as shown in Fig. 4($a_1$).

We then calculate the refractive index using the relation:

$$n(\omega) = \sqrt{\frac{|\varepsilon(\omega)| + \mathrm{Re}\,\varepsilon(\omega)}{2}}$$

The results are plotted in Fig. 4($a_2$). We see that the minimum value of the refractive index lies at a light wavelength of 116 nm, and the curve has gradual growth as wavelength increases and approaches the peak value of 1.5 at light wavelength of 306 nm in the ultraviolet region.

Since phosphorus and nitrogen are in the same group in the periodic table, we then carried out similar calculations on a g-$Si_3P_3$ sheet constructed by replacing N with P in the optimized structure of g-$Si_3N_3$. The fully optimized geometrical structure is plotted in Fig. 5. It also has a planar 2D hexagonal primitive cell but has a larger lattice constant of 10.70 Å, as compared to the g-$Si_3N_3$ sheet due to the bigger size of P atoms. The relaxed Si–Si and Si–P bond lengths are 2.35 Å and 2.16 Å, respectively. MD simulations confirm that the g-$Si_3P_3$ sheet is thermally stable at room temperature.

The electronic band structure of the g-$Si_3P_3$ is displayed in Fig. 6(a). It shows that the g-$Si_3P_3$ is a nonmagnetic semiconductor, while the silicene-like SiP sheet is metallic.[23] Different from the g-$Si_3N_3$ sheet, the g-$Si_3P_3$ sheet is a direct band gap semiconductor as both the VBM and CBM are located at the $K$ point

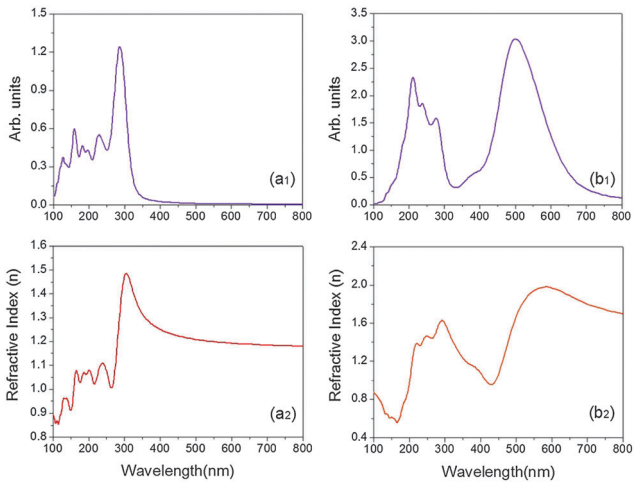


Fig. 4 Calculated optical absorptions ($a_1$) and ($b_1$), and refractive index ($a_2$) and ($b_2$) of the g-$Si_3N_3$ and g-$Si_3P_3$ sheets, respectively.

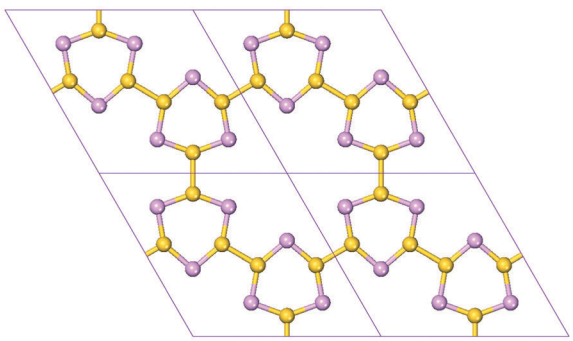

Fig. 5 Optimized structure of the g-$Si_3P_3$ sheet. Si and P atoms are represented by yellow and pink balls, respectively. The unit cells are marked by purple rhombus.

 

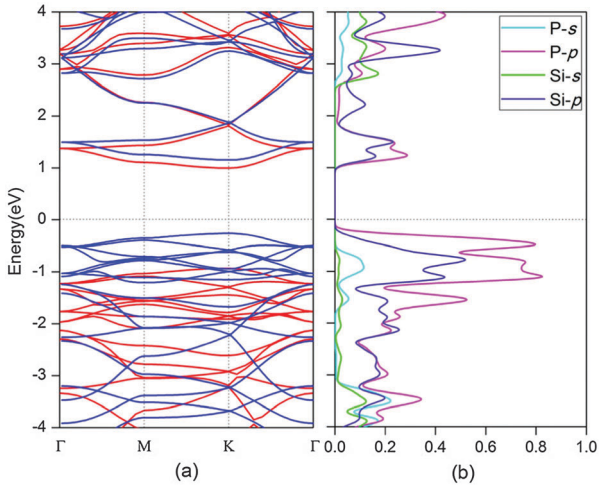


Fig. 6 (a) Electronic band structures of the g-$Si_3P_3$ using GGA-PBE (blue lines) and HSE06 hybrid functional (red lines). (b) PDOS of the g-$Si_3P_3$ at GGA-PBE level. The Fermi energy level is shifted to 0.00 eV.

in the Brillouin zone from both the GGA and HSE06 level calculations. The calculated band gap is 1.41 eV and 1.93 eV, respectively, from these two functionals. The corresponding PDOS of the g-$Si_3P_3$ is plotted in Fig. 6(b), showing that the VBM and CBM come from the p orbitals of both the Si and P atoms. For comparison, the optical absorption curve of g-$Si_3P_3$ is also given in Fig. 4($b_1$). We note, unlike the g-$Si_3N_3$, that the absorption curve of g-$Si_3P_3$ starts at about 100 nm with the first peak at 212 nm (corresponding photon energy is 5.9 eV) and the second peak at 501 nm (corresponding photon energy is 2.5 eV), namely, the absorption spectrum of the g-$Si_3P_3$ covers a wider range in visible light wavelength as compared to that of the g-$Si_3N_3$. Since the preferable energy window for photocatalytic materials is in the range of 400 to 770 nm, the g-$Si_3P_3$ would be suitable for solar absorbers. The calculated work function of g-$Si_3P_3$ is 5.57 eV, which is approximately the same value as a graphene sheet functionalized with OH groups,[32] showing its potential application in water-splitting. When excited by light, the electrons would jump into the conduction band enabling the reduction of $H_2O$ for $H_2$, while holes in the valance band would oxidize $H_2O$ for $O_2$. The calculated results of refractive index are also plotted in Fig. 4($b_2$), showing that the peak value of the g-$Si_3P_3$ shifts to the visible light range, which differs from the g-$Si_3N_3$.

In summary, a detailed first-principles DFT study on the stability, electronic and optical properties of the monolayer g-$Si_3N_4$, g-$Si_4N_3$, g-$Si_3N_3$ and g-$Si_3P_3$ sheets is performed. Their dynamical and thermal stabilities are examined by carrying out phonon calculations and MD simulations. The g-$Si_3N_3$ sheet is found to be stable, while the first two structures are dynamically unstable, indicating that the stability of 2D Si–N sheets can be manipulated by changing the stoichiometric ratio of Si : N. We find that unlike the previously studied silicene-like SiN and $Si_3N$ sheets which are metallic, the g-$Si_3N_3$ is semiconducting with an indirect band gap of 3.50 eV (at the HSE06 level). We have shown that the 2D sheet has a larger effective mass of holes, a smaller band gap, and a red shift of the optical absorption in ultraviolet wavelengths, as compared to the 3D $Si_3N_4$ structure, suggesting that in Si-based materials the electronic and optical properties can be tuned by changing dimensionality. When N is replaced by P forming a g-$Si_3P_3$ sheet, the system is also stable and becomes a semiconductor with a smaller energy direct band gap of 1.93 eV, as compared with the g-$Si_3N_3$ sheet. It has a main optical absorption peak at 501 nm in the visible light region, suggesting that the g-$Si_3P_3$ sheet may be a potential material for solar absorption. We hope that this work will provide some useful physical insights for experimental studies in this direction.

## Acknowledgements

This work was partially supported by grants from the National Natural Science Foundation of China (NSFC-11174014, NSFC-21273012), the National Grand Fundamental Research 973 Program of China (Grant No. 2012CB921404), and the Doctoral Program of Higher Education of China (20130001110033).

## References

1 K. S. Novoselov, A. K. Geim, S. V. Morozov, D. Jiang, Y. Zhang, S. V. Dubonos, I. V. Grigorieva and A. A. Firsov, *Science*, 2004, **306**, 666–669.
2 A. K. Geim and K. S. Novoselov, *Nat. Mater.*, 2007, **6**, 183–191.
3 A. Du, S. Sanvito and S. C. Smith, *Phys. Rev. Lett.*, 2012, **108**, 197207.
4 M. H. V. Huynh, M. A. Hiskey, J. G. Archuleta and E. L. Roemer, *Angew. Chem.*, 2005, **117**, 747–749.
5 X. Li, S. Zhang and Q. Wang, *Phys. Chem. Chem. Phys.*, 2013, **15**, 7142–7146.
6 P. Niu, G. Liu and H.-M. Cheng, *J. Phys. Chem. C*, 2012, **116**, 11013–11018.
7 P. Niu, L. Zhang, G. Liu and H. M. Cheng, *Adv. Funct. Mater.*, 2012, **22**, 4763–4770.
8 X. Wang, S. Blechert and M. Antonietti, *ACS Catal.*, 2012, **2**, 1596–1606.
9 X. Li, J. Zhou, Q. Wang, Y. Kawazoe and P. Jena, *J. Phys. Chem. Lett.*, 2013, **4**, 259–263.
10 Q. Guo, Q. Yang, C. Yi, L. Zhu and Y. Xie, *Carbon*, 2005, **43**, 1386–1391.
11 J. Li, C. Cao, J. Hao, H. Qiu, Y. Xu and H. Zhu, *Diamond Relat. Mater.*, 2006, **15**, 1593–1600.
12 G. Chai, C. Lin, M. Zhang, J. Wang and W. Cheng, *Nanotechnology*, 2010, **21**, 195702.
13 H. Qiu, Z. Wang and X. Sheng, *Phys. Lett. A*, 2013, **377**, 347–350.
14 Z. Ma, X. Zhao, Q. Tang and Z. Zhou, *Int. J. Hydrogen Energy*, 2014, **39**, 5037–5042.
15 M. Hoffmann, *Tailoring of mechanical properties of $Si_3N_4$ ceramics,* Springer, 1994, pp. 59–72.
16 R. N. Katz, *Science*, 1980, **208**, 841–847.
17 H. Lin and M. Ferber, *J. Eur. Ceram. Soc.*, 2002, **22**, 2789–2797.

18 D. Hardie and K. Jack, *Nature*, 1957, **180**, 332–333.
19 Y.-N. Xu and W. Ching, *Phys. Rev. B: Condens. Matter Mater. Phys.*, 1995, **51**, 17379.
20 G. Zhao and M. Bachlechner, *Phys. Rev. B: Condens. Matter Mater. Phys.*, 1998, **58**, 1887.
21 A. Zerr, G. Miehe, G. Serghiou, M. Schwarz, E. Kroke, R. Riedel, H. Fueß, P. Kroll and R. Boehler, *Nature*, 1999, **400**, 340–342.
22 J. Leger, J. Haines, M. Schmidt, J. Petitet, A. Pereira and J. Da Jornada, *Nature*, 1996, **383**, 401.
23 Y. Ding and Y. Wang, *J. Phys. Chem. C*, 2013, **117**, 18266–18278.
24 G. Kresse and J. Furthmüller, *Phys. Rev. B: Condens. Matter Mater. Phys.*, 1996, **54**, 11169.
25 J. P. Perdew, K. Burke and M. Ernzerhof, *Phys. Rev. Lett.*, 1996, **77**, 3865.
26 J. Heyd, G. E. Scuseria and M. Ernzerhof, *J. Chem. Phys.*, 2003, **118**, 8207–8215.
27 H. J. Monkhorst and J. D. Pack, *Phys. Rev. B: Solid State*, 1976, **13**, 5188–5192.
28 A. Togo, F. Oba and I. Tanaka, *Phys. Rev. B: Condens. Matter Mater. Phys.*, 2008, **78**, 134106.
29 D. Jose and A. Datta, *J. Phys. Chem. C*, 2012, **116**, 24639–24648.
30 S. Cahangirov, M. Topsakal, E. Aktürk, H. Şahin and S. Ciraci, *Phys. Rev. Lett.*, 2009, **102**, 236804.
31 S. Nosé, *J. Chem. Phys.*, 1984, **81**, 511–519.
32 X. Jiang, J. Nisar, B. Pathak, J. Zhao and R. Ahuja, *J. Catal.*, 2013, **299**, 204–209.
33 W. Clegg, M. Noltemeyer, G. M. Sheldrick and N. Vater, *Acta Crystallogr., Sect. B: Struct. Crystallogr. Cryst. Chem.*, 1980, **36**, 2461–2462.
34 W. Clegg, G. M. Sheldrick and D. Stalke, *Acta Crystallogr., Sect. C: Cryst. Struct. Commun.*, 1984, **40**, 816–818.
35 A. Du, S. Sanvito, Z. Li, D. Wang, Y. Jiao, T. Liao, Q. Sun, Y. H. Ng, Z. Zhu and R. Amal, *J. Am. Chem. Soc.*, 2012, **134**, 4393–4397.
36 F. Wu, Y. Liu, G. Yu, D. Shen, Y. Wang and E. Kan, *J. Phys. Chem. Lett.*, 2012, **3**, 3330–3334.

 